Direct Model Predictive Control with an Extended Prediction Horizon for Quasi-Z-Source Inverters

Ayman Ayad, Petros Karamanakos, and Ralph Kennel
Institute of Electrical Drive Systems and Power Electronics, Technische Universität München, Munich, Germany
Email: ayman.francees@tum.de, p.karamanakos@ieee.org, ralph.kennel@tum.de

***Abstract*—This paper presents a direct model predictive control (MPC) with an extended prediction horizon for the quasi-Z-source inverter (qZSI). The proposed MPC controls both sides of the qZSI based on the inductor current of the qZS network and the output current of the ac side. In order to improve the system performance, the MPC with extended prediction horizon is used. However, increasing the prediction horizon results in a huge increase in the computational burden which prevents the implementation of the MPC in real time. To solve this problem, two techniques are utilized, namely a branch-and-bound scheme and move blocking strategy. In this work, the discrete-time model of the qZSI is derived that accurately captures all operating modes and states. Then, the steady-state and transient operations of the qZSI with the proposed MPC are experimentally examined. The results confirm that by extending the prediction horizon, the qZSI behavior is significantly improved.**

I. Introduction

In the last few decades renewable energy systems (RES), most notably wind energy and photovoltaic (PV) have dramatically grown up and become important energy sources for the whole world [1]. However, the output voltage of PV is variable since it depends on the temperature and the solar irradiation level. Thus, power electronic converters are used in order to feed the loads/grid with a fixed and regulated ac power. The PV commonly employs voltage source inverters (VSIs) as dc-ac converters [2]. However, when the PV voltage is not sufficient to generate the required ac current/voltage, an additional dc-dc boost converter is required to boost the input voltage to the required dc-link voltage. The dc-dc boost converter increases the controller complexity and the system cost. In addition, it decreases the overall efficiency of the converter [3].

Recently, impedance-source inverters have been paid much attention from the researchers in the area of power electronics as alternative to the conventional two-stage inverters [4], [5]. These inverters are considered as one-stage buck-boost converters by using an impedance network and including an extra switching state, defined as shoot-through state. The first topology of the impedance-source inverters is called Z-source inverter (ZSI) [6]. However, the quasi-Z-source inverter (qZSI) [7], a modified version of the ZSI, has been widely used with the RES, especially with PV generation systems [8], [9]. In comparison with the ZSI, the qZSI draws a continuous input current, requires smaller passive components, and provides a common earthing between the PV and the dc-link bus [10]. Thus, the qZSI is considered as an attractive solution for PV systems. In order to assure the system stability, both dc and ac sides of the qZSI have to be simultaneously controlled. The dc-side controller manages the boost operation, while the ac-side controller achieves the dc-ac conversion.

One of the most promising control techniques that has been recently applied on wide range of power electronic applications is the direct MPC, also referred to as a finite control set (FCS) MPC [11]–[13]. The MPC is easy to be implemented, can handle multiple control objectives, manipulates the converter switches without a necessity for a modulator, and introduces a very fast dynamic response [12], [14]. Considering these advantages, the MPC with a single-step prediction is also applied on the qZSI [15]–[17]. However, the single-step is not always sufficient for the qZSI to exhibit a satisfactory performance, particularly when the switching frequency is relatively low. A long-horizon MPC for the qZSI is introduced in [18]; however, only simulations were provided only with the boost mode operation.

This paper introduces the MPC with extended prediction horizon for the qZSI. The proposed method is experimentally validated for both modes of operation, namely buck and boost mode. First, a discrete-time model of the converter is derived, on which the controller relies to accurately predict the future behavior of the system over the whole operating regime. Hence, the proposed MPC scheme is applicable to both operating modes of the converter. Moreover, in order to reduce the required number of calculations and allow the implementation of the MPC in real time, a branch and bound technique [19] along with a move blocking strategy [20] are employed.

II. Mathematical Model of Quasi-Z-Source Inverter

The three-phase qZSI connected with an RL load is shown in Fig. 1. The qZSI consists of a quasi-Z-source (qZS) network and a two-level inverter. The qZSI has two modes of operation, namely buck and boost mode. In buck mode, the dc-link voltage is roughly equal to the input voltage, where the qZSI works as the conventional VSI. In boost mode, an extra switching state (shoot-through state) is included by which the dc-link voltage can be boosted to the desired level. Thus, the switching states of the qZSI in boost mode can be categorized into two types, namely the non-shoot-through and shoot-through state as illustrated in Fig. 2.

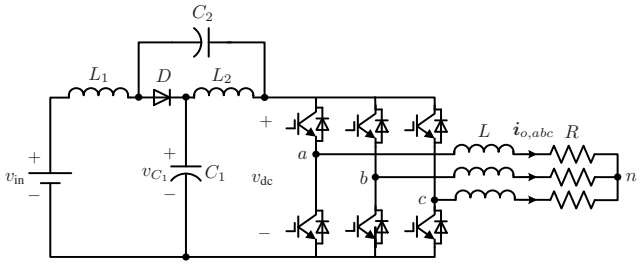

Fig. 1: Topology of the quasi-Z-source inverter (qZSI).

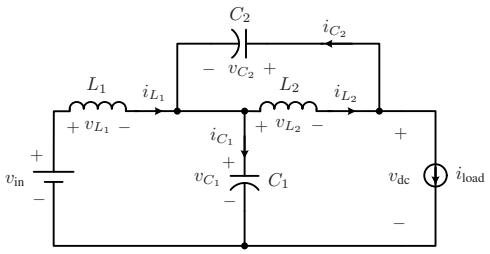

(a) Non-shoot-through state.

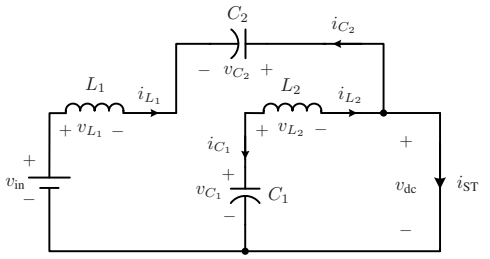

(b) Shoot-through state.

Fig. 2: Operation states of the qZSI during the boost mode.

For the system under investigation, the state vector includes the output current[1], the inductor currents, and the capacitor voltages, i.e. $\boldsymbol{x} = [i_{o,\alpha}\ i_{o,\beta}\ i_{L_1}\ i_{L_2}\ v_{C_1}\ v_{C_2}]^T \in \mathbb{R}^6$. The output and the inductor currents compose the output vector, i.e. $\boldsymbol{y} = [i_{o,\alpha}\ i_{o,\beta}\ i_{L_1}]^T \in \mathbb{R}^3$. Moreover, the system input are the three-phase switching positions $\boldsymbol{u}_{abc} \in \mathcal{U}^3$, where $\boldsymbol{u}_{abc} = [u_a\ u_b\ u_c]^T$ and $\mathcal{U} = \{0, 1\}$. Finally, the input voltage is considered as a disturbance to the system, i.e. $\boldsymbol{w} = v_{\text{in}} \in \mathbb{R}$. Note that the physical model of the qZSI will be separately derived for each operating mode and state. Then, the overall model of the system will be obtained.

A. Operation in Boost Mode

During the non-shoot-through state, as shown in Fig. 2(a), the input voltage source and the inductors charge the capacitors and feed the load. In this case, the three-phase inverter is represented by a constant current source i_{load}. Accordingly, the converter model is obtained by

$$\frac{\mathrm{d}\boldsymbol{x}(t)}{\mathrm{d}t} = \boldsymbol{F}_1\boldsymbol{x}(t) + \boldsymbol{G}\boldsymbol{u}_{abc}(t) + \boldsymbol{H}\boldsymbol{w}(t)\,, \quad \boldsymbol{y}(t) = \boldsymbol{E}\boldsymbol{x}(t)\,, \quad (1)$$

[1]To ease the computations it is common practice to express a variable in the stationary orthogonal system $(\alpha\beta)$ instead of the three-phase system (abc), i.e. $\boldsymbol{\xi}_{\alpha\beta} = \boldsymbol{K}\boldsymbol{\xi}_{abc}$, where $\boldsymbol{K}$ is the transformation matrix of appropriate dimensions. Note, though, that, the subscript for vectors in the $\alpha\beta$ plane is dropped within the text to simplify the notation. Vectors in the abc plane are denoted with the corresponding subscript.

where matrices $\boldsymbol{F}_1$, $\boldsymbol{G}$, $\boldsymbol{H}$ and $\boldsymbol{E}$ can be found in Section II in [18].

As shown in Fig. 2(b), during the shoot-through state, the diode is off and the load is short-circuited. During this state, the input voltage source and the capacitors charge the inductors. Consequently, the model is given by

$$\frac{\mathrm{d}\boldsymbol{x}(t)}{\mathrm{d}t} = \boldsymbol{F}_2\boldsymbol{x}(t) + \boldsymbol{G}\boldsymbol{u}_{abc}(t) + \boldsymbol{H}\boldsymbol{w}(t)\,, \quad \boldsymbol{y}(t) = \boldsymbol{E}\boldsymbol{x}(t)\,, \quad (2)$$

where $\boldsymbol{F}_2$ is given in [18] (see Section II).

B. Operation in Buck Mode

In buck mode, the qZSI operates as the conventional VSI. Thus, only the ac side of qZSI is considered for the system model as follows

$$\frac{\mathrm{d}\boldsymbol{x}(t)}{\mathrm{d}t} = \boldsymbol{F}_3\boldsymbol{x}(t) + \boldsymbol{G}\boldsymbol{u}_{abc}(t)\,, \quad \boldsymbol{y}(t) = \boldsymbol{E}\boldsymbol{x}(t)\,, \quad (3)$$

where the only nonzero entries of $\boldsymbol{F}_3$ are the two first diagonal entries (i.e. $\boldsymbol{F}_{3_{(1,1)}}$ and $\boldsymbol{F}_{3_{(2,2)}}$) which are equal to $-R/L$, with R and L being the load resistance and inductance, respectively.

C. Continuous-Time Model

The derived models (1), (2) and (3) can compose one model that precisely describes the different operating modes and states of the qZSI. To do so, two auxiliary binary variables d_{aux_1} and d_{aux_2} are introduced. Variable d_{aux_1} indicates the state at which the converter operates when in boost mode, i.e.

$$d_{\text{aux}_1} = \begin{cases} 0 & \text{if non-shoot-through state} \\ 1 & \text{if shoot-through state} \end{cases}. \quad (4)$$

Variable d_{aux_2} is used to indicate the operation mode, i.e.

$$d_{\text{aux}_2} = \begin{cases} 0 & \text{if buck mode (i.e. } i_o \leq i_{o,\text{bnd}}) \\ 1 & \text{if boost mode (i.e. } i_o > i_{o,\text{bnd}}) \end{cases}. \quad (5)$$

where the transition from the buck mode to the boost mode (and vice versa) depends on whether the output current becomes greater (less) than the current $i_{o,\text{bnd}}$ that defines the boundary between the two modes, see the appendix.

Taking all the above into account, the model of the converter can be written as

$$\frac{\mathrm{d}\boldsymbol{x}(t)}{\mathrm{d}t} = \boldsymbol{F}\boldsymbol{x}(t) + \boldsymbol{G}\boldsymbol{u}_{abc}(t) + d_{\text{aux}_2}\boldsymbol{H}\boldsymbol{w}(t)\,, \quad \boldsymbol{y}(t) = \boldsymbol{E}\boldsymbol{x}(t)\,, \quad (6)$$

where $\boldsymbol{F} = \boldsymbol{F}_a + d_{\text{aux}_2}\boldsymbol{F}_b$, with $\boldsymbol{F}_a = \boldsymbol{F}_3$ and

$$\boldsymbol{F}_b = \begin{bmatrix} -\frac{R}{L} & 0 & 0 & 0 & 0 & 0 \\ 0 & -\frac{R}{L} & 0 & 0 & 0 & 0 \\ 0 & 0 & 0 & 0 & \frac{d_{\text{aux}_1}-1}{L_1} & \frac{d_{\text{aux}_1}}{L_1} \\ 0 & 0 & 0 & 0 & \frac{d_{\text{aux}_1}}{L_2} & \frac{d_{\text{aux}_1}-1}{L_2} \\ \frac{m_1}{C_1} & \frac{m_2}{C_1} & \frac{1-d_{\text{aux}_1}}{C_1} & -\frac{d_{\text{aux}_1}}{C_1} & 0 & 0 \\ \frac{m_1}{C_2} & \frac{m_2}{C_2} & -\frac{d_{\text{aux}_1}}{C_2} & \frac{1-d_{\text{aux}_1}}{C_2} & 0 & 0 \end{bmatrix}$$

where [2]

$$m_1 = (d_{\text{aux}_1} - 1)\boldsymbol{u}_{abc}^T\boldsymbol{K}_{(:,1)}^{-1}, \quad m_2 = (d_{\text{aux}_1} - 1)\boldsymbol{u}_{abc}^T\boldsymbol{K}_{(:,2)}^{-1}$$

Fig. 3 shows the qZSI represented as an automaton, where the auxiliary variables d_{aux_1} and d_{aux_2} define the transition from one state to another.

[2]For a matrix $\boldsymbol{M}$, $\boldsymbol{M}_{(:,i)}$ represents its ith column.

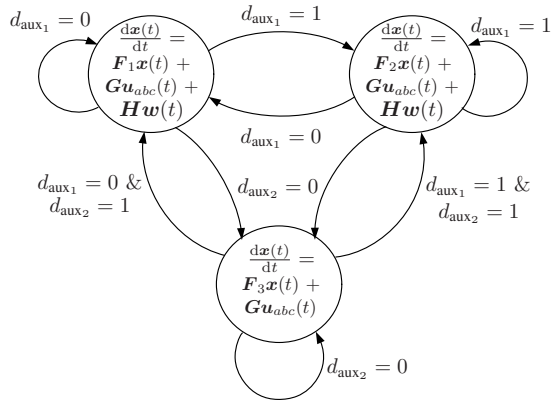

Fig. 3: The qZSI presented as a continuous-time automaton.

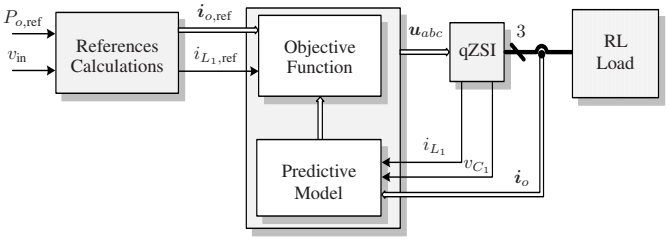

Fig. 4: Proposed MPC with reference tracking for the qZSI.

III. Direct Model Predictive Current Control of qZSI

The proposed MPC aims to regulate the output and the inductor currents along their reference values. In addition, the switching frequency is to be kept relatively low in order to reduce the switching losses. The proposed direct MPC with extended horizon for qZSI is demonstrated in Fig. 4. It consists of two main parts: the predictive model, and the objective function. As a first step, the MPC calculates the future predictions of the controlled variables over a finite prediction horizons based on the system model as well as the present measurements of the output current, inductor current, and capacitor voltage. Then, the optimal switching state is selected by minimizing the objective function in real time.

A. Discrete-Time Controller Model

The proposed MPC requires the discrete-model of the system in order to compute the variables predictions. To do that, the continuous-time model (6) is discretized using forward Euler approximation as follows

$$\boldsymbol{x}(k+1) = \boldsymbol{A}\boldsymbol{x}(k) + \boldsymbol{B}\boldsymbol{u}_{abc}(k) + \boldsymbol{D}\boldsymbol{w}(k)\,, \quad \boldsymbol{y}(k) = \boldsymbol{C}\boldsymbol{x}(k)\,, \quad (7)$$

where $\boldsymbol{A} = (\boldsymbol{F} + \boldsymbol{I})T_s$, $\boldsymbol{B} = \boldsymbol{G}T_s$, $\boldsymbol{D} = \boldsymbol{H}T_s$ and $\boldsymbol{C} = \boldsymbol{E}$. In addition, $\boldsymbol{I}$ is the identity matrix, T_s denotes the sampling interval, and $k \in \mathbb{N}$.

B. Optimal Control Problem

In order to minimize the error between the reference and the predicted values of the output and the inductor currents, and to control the switching effort over a finite prediction horizon of N, the objective function is chosen as

$$J(k) = \sum_{\ell=k}^{k+N-1} ||\boldsymbol{y}_{\text{ref}}(\ell{+}1|k) - \boldsymbol{y}(\ell{+}1|k)||^2_{\boldsymbol{Q}} + ||\Delta\boldsymbol{u}_{abc}(\ell|k)||^2_{\boldsymbol{R}}\,, \quad (8)$$

where $\boldsymbol{y}_{\text{ref}} = [i_{o,\alpha,\text{ref}}\ i_{o,\beta,\text{ref}}\ i_{L_1,\text{ref}}]^T$ and $\Delta\boldsymbol{u}_{abc}(k) = \boldsymbol{u}_{abc}(k) - \boldsymbol{u}_{abc}(k-1)$. The second term is added to adjust the switching frequency of the qZSI. Moreover, the diagonal, positive semidefinite matrices $\boldsymbol{Q}$ and $\boldsymbol{R} \in \mathbb{R}^{3\times3}$ are the weighting matrices[3] that set the trade-off between the system tracking accuracy and the converter switching efforts. The optimal switching sequence over the horizon $\boldsymbol{U}^*(k) = [{\boldsymbol{u}^*_{abc}}^T(k)\ {\boldsymbol{u}^*_{abc}}^T(k+1) \dots {\boldsymbol{u}^*_{abc}}^T(k+N-1)]^T$ is calculated by minimizing the objective function (8), where only the first element of $\boldsymbol{U}^*(k)$ is applied to the qZSI. Then, the whole process is reaped at each time-step with new measurements.

C. Reducing the Computational Complexity

Increasing the prediction horizon results in a better system performance. However, the computational demand of the MPC is exponentially increases (8^N, with N being the number of the prediction steps) which prohibits its implementation in real time. For instance, with MPC with three-step prediction horizon, the required number of calculations is $8^3 = 512$. However, by adopting a branch-and-bound technique [19] and a move blocking scheme [20], [21], the computational burden can be significantly reduced. These techniques are explained in detail for the present application in a previous work [18].

IV. Experimental Evaluation

Experiments with the proposed MPC strategy were carried out in the laboratory to examine the performance of the qZSI (shown in Fig. 1) in both buck and boost modes. The system parameters are chosen as $v_{\text{in}} = 70\,\text{V}$, $L_1 = L_2 = 1\,\text{mH}$, $C_1 = C_2 = 480\,\mu\text{F}$, $R = 10\,\Omega$, and $L = 10\,\text{mH}$. Based on the reference output power ($P_{o,\text{ref}} = 315\,\text{W}$), the output current reference $\boldsymbol{i}_{o,\text{ref}}$ is set to $4\,\text{A}$, while the inductor current reference is equal to $4.5\,\text{A}$ ($i_{L_1,\text{ref}} = P_{o,\text{ref}}/v_{\text{in}}$). The sampling interval is $T_s = 20\,\mu\text{s}$. Throughout the upcoming experiments, the qZSI operates at the desired switching frequency $f_{\text{sw}} = 10\,\text{kHz}$, by adjusting $\boldsymbol{Q} = \text{diag}(1, 1, 0.8)$ and $\boldsymbol{R} = \lambda_u\boldsymbol{I}$ in (8), where $\lambda_u > 0$ is appropriately tuned.

A. Steady-State Operation

The steady-state behavior of the qZSI when operated at $10\,\text{kHz}$ switching frequency is examined. The proposed MPC is tested with two different prediction horizon lengths ($1T_s$ and $3T_s$), where the λ_u is chosen as 0.5 and 0.4, respectively.

The experimental dc- and ac-side results are shown in Figs. 5, 6, 7 and 8 for MPC with $1T_s$ and $3T_s$, respectively. With regard to the dc side, it can be observed that the inductor current effectively tracks its reference in both examined cases

[3]The squared norm weighted with the positive (semi)definite matrix $\boldsymbol{W}$ is given by $||\boldsymbol{\xi}||^2_{\boldsymbol{W}} = \boldsymbol{\xi}^T\boldsymbol{W}\boldsymbol{\xi}$.

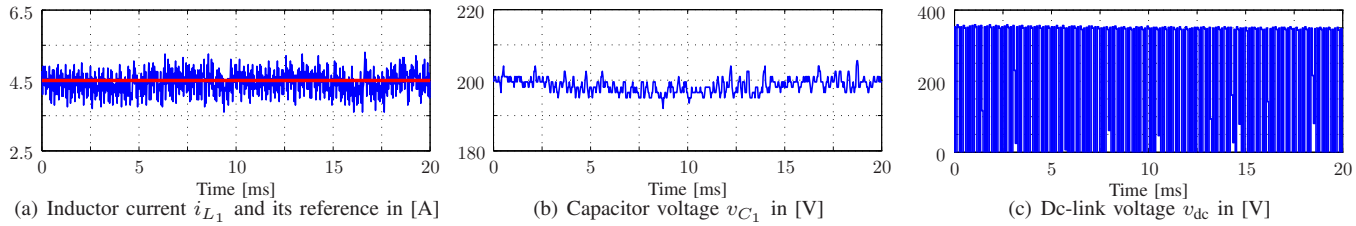

(a) Inductor current i_{L_1} and its reference in [A] (b) Capacitor voltage v_{C_1} in [V] (c) Dc-link voltage v_{dc} in [V]

Fig. 5: Experimental results of the dc side of the qZSI with MPC and an $1T_s$ prediction horizon length. The sampling interval is $T_s = 20\,\mu$s and $\lambda_u = 0.5$. The switching frequency is $f_{\text{sw}} \approx 10$ kHz.

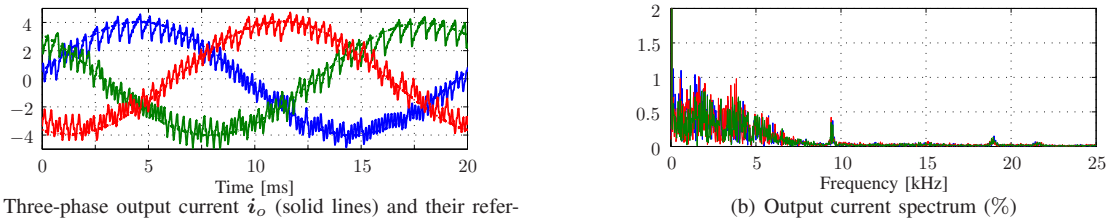

(a) Three-phase output current $\boldsymbol{i}_o$ (solid lines) and their references (dash-dotted lines) in [A] (b) Output current spectrum (%)

Fig. 6: Experimental results of the ac side of the qZSI with MPC and an $1T_s$ prediction horizon length. The sampling interval is $T_s = 20\,\mu$s and $\lambda_u = 0.5$. The switching frequency is $f_{\text{sw}} \approx 10$ kHz and the output current THD $I_{o,\text{THD}} = 8.36\%$.

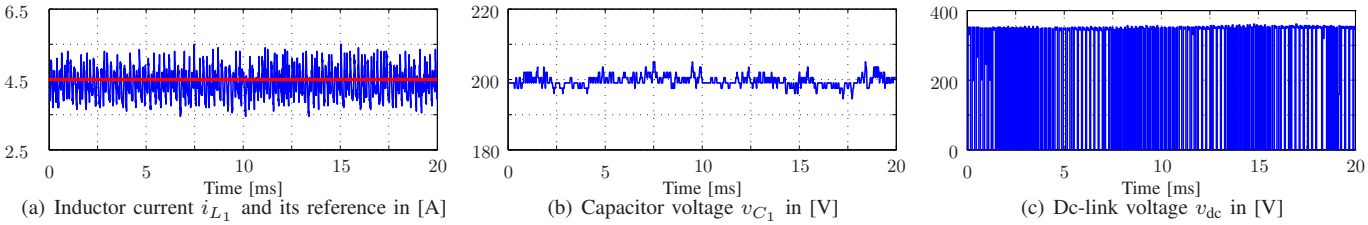

(a) Inductor current i_{L_1} and its reference in [A] (b) Capacitor voltage v_{C_1} in [V] (c) Dc-link voltage v_{dc} in [V]

Fig. 7: Experimental results of the dc side of the qZSI with MPC and a $3T_s$ prediction horizon length. The sampling interval is $T_s = 20\,\mu$s and $\lambda_u = 0.4$. The switching frequency is $f_{\text{sw}} \approx 10$ kHz.

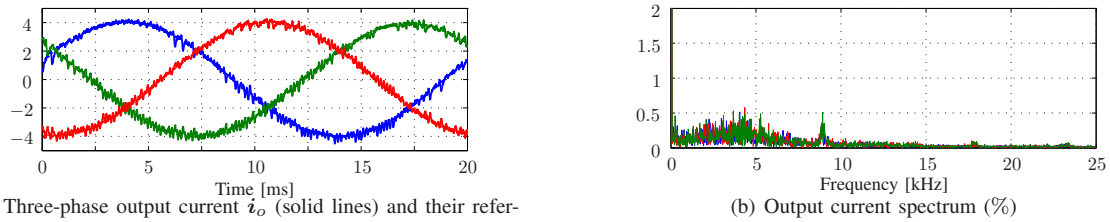

(a) Three-phase output current $\boldsymbol{i}_o$ (solid lines) and their references (dash-dotted lines) in [A] (b) Output current spectrum (%)

Fig. 8: Experimental results of the ac side of the qZSI with MPC and a $3T_s$ prediction horizon length. The sampling interval is $T_s = 20\,\mu$s and $\lambda_u = 0.4$. The switching frequency is $f_{\text{sw}} \approx 10$ kHz and the output current THD $I_{o,\text{THD}} = 2.92\%$.

(Figs. 5(a) and 7(a)), resulting in a boosted capacitor voltage $v_{C_1} = 200$ V (Figs. 5(b) and 7(b)) and a peak dc-link voltage of $\hat{v}_{\text{dc}} = 350$ V (Figs. 5(c) and 7(c)). Regardless of the prediction horizon length, the MPC shows good steady-state behavior for the dc side of the qZSI. However, the MPC with $3T_s$ exhibits a better behavior.

On the ac side of the qZSI, as can be seen in Figs. 6(a) and 8(a), the output current is well tracked. However, the MPC with a $3T_s$ prediction interval produces current THD of 2.92% (see Fig. 8(b)), remarkably lower than the THD with the $1T_s$ horizon MPC (8.36%), see Fig. 6(b). This concludes that increasing the prediction horizon notably enhances the overall performance of the qZSI.

The computational demands of the proposed MPC for both modes of operation of the qZSI are also investigated. Table I shows the numbers of the complete switching sequences μ and nodes ν examined when the qZSI operates in buck and boost mode as a function of the prediction horizon length. For comparison purposes, the number of the switching sequences evaluated with the exhaustive enumeration algorithm is also illustrated. The results show that by using a branch-and-bound strategy and a move blocking scheme, the calculation effort is remarkably decreased. For instance, with a prediction length of 3 time steps, the maximum number of the switching sequences is reduced by about 89% and 92% for buck and boost mode, respectively. The reduction in the calculation effort allows the real time implementation of the MPC. Moreover, the output current THD values confirm that the MPC with longer prediction horizons improves the performance of the qZSI.

Furthermore, some experiments were conducted to study the trade-off between the current THD and the switching frequency of the proposed MPC strategy with prediction intervals equal to $1T_s$, $2T_s$ and $3T_s$. For all cases examined, λ_u was appropriately tuned to obtain the desired switching

TABLE I: The average and the maximum numbers of the examined switching sequences μ and nodes ν depending on the length of the prediction horizon for buck and boost modes of the qZSI with the obtained output current THD at $f_{\text{sw}} \approx 10\,\text{kHz}$.

Operating Mode	Length of Prediction Horizon $NT_s = (N_1 + n_s N_2)T_s$	Exhaustive Search			Proposed MPC Strategy					THD %
		$N_1 + N_2$	μ	ν	$N_1 + N_2$	avg(μ)	avg(ν)	max(μ)	max(ν)	
Buck mode	1	$1+0$	7	7	$1+0$	7	7	7	7	12.90
	2	$2+0$	49	56	$2+0$	16	23.8	28	32	4.83
	3	$3+0$	343	399	$1+1$	22.6	27.8	35	41	3.02
Boost mode	1	$1+0$	8	8	$1+0$	8	8	8	8	8.36
	2	$2+0$	64	72	$2+0$	22.1	33.5	32	44	3.96
	3	$3+0$	512	584	$1+1$	27.4	38.3	40	47	2.92

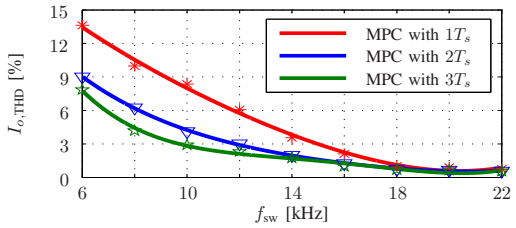

Fig. 9: Trade-off between the current THD $I_{o,\text{THD}}$ and the switching frequency f_{sw} for the MPC with prediction horizon length of $1T_s$, $2T_s$ and $3T_s$.

frequency. The results are approximated by a fourth degree polynomial and illustrated in Fig. 9. Among the different prediction horizons, it can be noticed that MPC with a $3T_s$ horizon introduces the lowest THD values over the whole range of switching frequencies.

B. Transient Response

The transient response of the proposed MPC strategy is examined with a $3T_s$ horizon and a switching frequency of $\approx 10\,\text{kHz}$. Two different cases of step changes are scrutinized: step change in the output current reference, and step change in the input dc voltage.

In the first case, the output current is stepped up from 2 A (buck mode) to 4 A (boost mode). Accordingly, the inductor current reference changes from 1.8 A to 4.5 A. The dc- and ac-side results are shown in Fig. 10. As can be seen in Fig. 10(a), the inductor current tracks its reference both before and after the change in its reference value, i.e. both in buck and boost modes, see also Fig. 11(a) where the transient is depicted in more detail. This is thanks to the discrete-time model of the converter, derived in Section II, which allows for the controller to accurately predict the system behavior not only over a limited range of operating points, but rather over the whole operating regime. As for the ac side, the proposed MPC manages to eliminate the steady-state error (Fig. 10(c)), with a very short transient time as shown in Fig. 11(b).

In the second experiment, the proposed MPC is investigated under step change in the input voltage. More specifically, the input voltage v_{in} is stepped up from 70 V to 100 V. Consequently, the inductor current reference is decreased from 4.5 A to 3.15 A. The experimental results for both sides of the qZSI are shown in Fig. 12. As can be observed in Fig. 12(a), the inductor current perfectly tracks its reference which in turn leads to a reduction in the capacitor voltage from 200 V to 150 V (see Fig. 12(b)). On the ac side, the output current is efficiently regulated along its reference value (see Fig. 12(c)). Both the inductor and output currents have very short transient times. These results show the effectiveness of the proposed MPC in handling the transient response with superior tracking abilities.

V. Conclusions

This work proposes a direct MPC for the qZSI for PV applications. To achieve an improved system performance, as quantified by the output current THD, long prediction horizons are required. However, solving the optimization problem in real time is such a case becomes computationally prohibitive. To overcome this problem, two techniques are utilized in this work, namely a branch-and-bound scheme and move blocking strategy. The paper first drives the discrete-time model that defines all operating modes and states of the qZSI. Then, the steady-state and transient operation of the qZSI are experimentally investigated. The results show that the proposed MPC strategy offers a very good steady-state behavior as well as very fast dynamic responses during transients.

Appendix

The output power P_o of the qZSI can be calculated by $P_o = 3\,v_o\,i_o\cos\varphi$, where v_o (i_o) is the output voltage (current) and $\cos\varphi$ is the system power factor. For the qZSI v_o can be written as

$$v_o = \frac{1}{2\sqrt{2}}\,m\,\hat{v}_{\text{dc}} = \frac{1}{2\sqrt{2}}\,\frac{1}{1-2d}\,m\,v_{\text{in}}\,, \tag{9}$$

where m is the inverter modulation index, d is the *average* shoot-through duty cycle, and $\hat{v}_{\text{dc}}$ denotes the peak dc-link voltage, see the appendix in [18]. Considering that the simple boost control method is used (also utilized with PI control [9]), m can be expressed by d, i.e. $m = 1 - d$. This results in

$$v_o = \frac{1}{2\sqrt{2}}\,\frac{1-d}{1-2d}\,v_{\text{in}} \tag{10}$$

Then,

$$P_o = \frac{3}{2\sqrt{2}}\,\frac{1-d}{1-2d}\,v_{\text{in}}\,i_o\,\cos\varphi \tag{11}$$

The boost function b_f can be deduced from (11) as

$$b_f = \frac{1-d}{1-2d} = \frac{2\sqrt{2}}{3}\,\frac{P_o}{v_{\text{in}}\,i_o\,\cos\varphi} \tag{12}$$

If $b_f > 1$, then the shoot-through duty cycle d is more than zero which means that the converter should work in boost mode in order to generate the required output current. On the other hand, $b_f \leq 1$ indicates that the converter should work

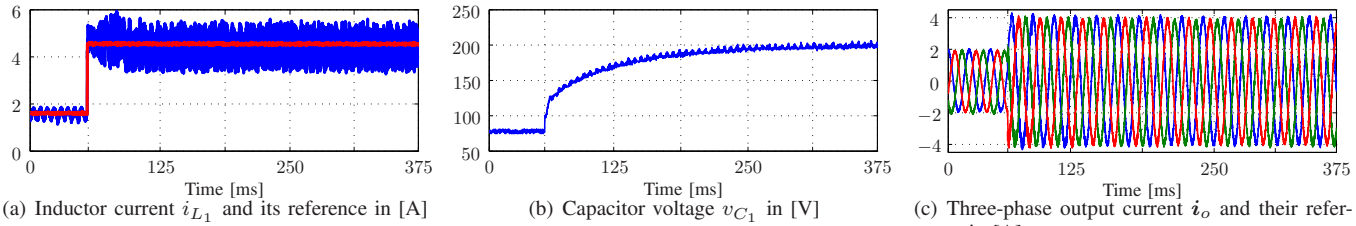

(a) Inductor current i_{L_1} and its reference in [A] (b) Capacitor voltage v_{C_1} in [V] (c) Three-phase output current $\boldsymbol{i}_o$ and their references in [A]

Fig. 10: Experimental results for a step change in the output current reference with MPC and a $3T_s$ prediction horizon length.

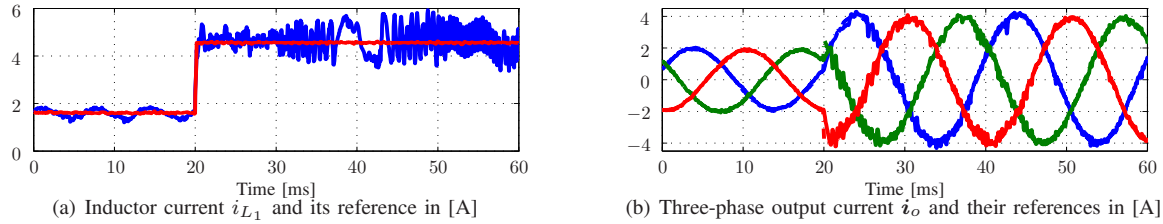

(a) Inductor current i_{L_1} and its reference in [A] (b) Three-phase output current $\boldsymbol{i}_o$ and their references in [A]

Fig. 11: Zoomed-in experimental results of the inductor and output currents for a step change in the output current reference with MPC.

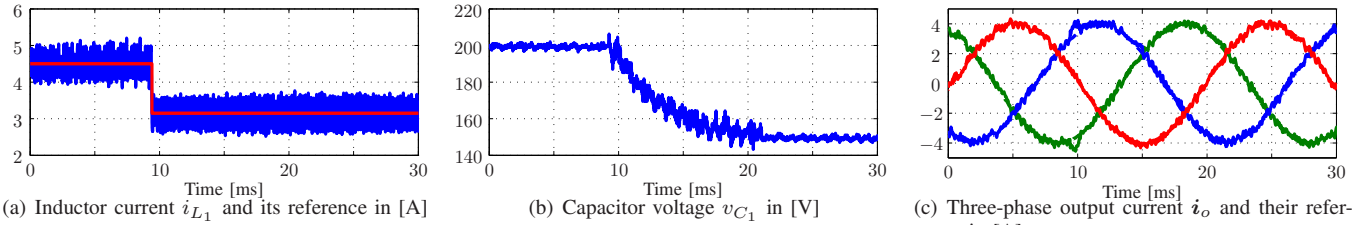

(a) Inductor current i_{L_1} and its reference in [A] (b) Capacitor voltage v_{C_1} in [V] (c) Three-phase output current $\boldsymbol{i}_o$ and their references in [A]

Fig. 12: Experimental results for a step change in the input voltage with MPC and a $3T_s$ prediction horizon length.

in buck mode. The output power can also be computed by $P_o = 3\, i_o^2\, R$. Thus, the current $i_{o,\text{bnd}}$ that defines the boundary between the two modes can be written as

$$i_{o,\text{bnd}} = \frac{v_{\text{in}}\, \cos\varphi}{2\sqrt{2}\, R}\,. \tag{13}$$

REFERENCES

[1] L. Hirth, "Market value of solar power: Is photovoltaics cost-competitive?" *IET Renewable Power Generation*, vol. 9, no. 1, pp. 37–45, Jan. 2015.

[2] S. B. Kjaer, J. K. Pedersen, and F. Blaabjerg, "A review of single-phase grid-connected inverters for photovoltaic modules," *IEEE Trans. Ind. Appl.*, vol. 41, no. 5, pp. 1292–1306, Sep./Oct. 2005.

[3] T. F. Wu, C. H. Chang, L. C. Lin, and C. L. Kuo, "Power loss comparison of single- and two-stage grid-connected photovoltaic systems," *IEEE Trans. Energy Convers.*, vol. 26, no. 2, pp. 707–715, Jun. 2011.

[4] A. Ayad, M. Ismeil, R. Kennel, and M. Orabi, "Experimental studies on a single-phase improved switched inductor Z-source inverter," in *Proc. Eur. Power Electron. Conf.*, Lille, France, Sep. 2013, pp. 1–10.

[5] Y. Siwakoti, F. Z. Peng, F. Blaabjerg, P. C. Loh, and G. Town, "Impedance-source networks for electric power conversion part I: A topological review," *IEEE Trans. Power Electron.*, vol. 30, no. 2, pp. 699–716, Feb. 2015.

[6] F. Z. Peng, "Z-source inverter," *IEEE Trans. Ind. Appl.*, vol. 39, no. 2, pp. 504–510, 2003.

[7] J. Anderson and F. Peng, "Four quasi-Z-source inverters," in *Proc. IEEE Power Electron. Spec. Conf.*, Rhodes, Greece, Jun. 2008, pp. 2743–2749.

[8] Y. Li, S. Jiang, J. Cintron-Rivera, and F. Z. Peng, "Modeling and control of quasi-Z-source inverter for distributed generation applications," *IEEE Trans. Ind. Electron.*, vol. 60, no. 4, pp. 1532–1541, Apr. 2013.

[9] A. Ayad, S. Hanafiah, and R. Kennel, "A comparison of quasi-Z-source inverter and traditional two-stage inverter for photovoltaic application," in *Proc. Int. Expo. and Conf. Power Electron., Intelligent Motion, Renew. Energy Management*, Nuremberg , Germany, May 2015, pp. 1–8.

[10] B. Ge, H. Abu-Rub, F. Z. Peng, Q. Lei, A. de Almeida, and F. Ferreira, "An energy-stored quasi-Z-source inverter for application to photovoltaic power system," *IEEE Trans. Ind. Electron.*, vol. 60, no. 10, pp. 4468–4481, Oct. 2013.

[11] P. Cortés, M. P. Kazmierkowski, R. M. Kennel, D. E. Quevedo, and J. Rodríguez, "Predictive control in power electronics and drives," *IEEE Trans. Ind. Electron.*, vol. 55, no. 12, pp. 4312–4324, Dec. 2008.

[12] J. Rodríguez, M. P. Kazmierkowski, J. R. Espinoza, P. Zanchetta, H. Abu-Rub, H. A. Young, and C. A. Rojas, "State of the art of finite control set model predictive control in power electronics," *IEEE Trans. Ind. Informat.*, vol. 9, no. 2, pp. 1003–1016, May 2013.

[13] P. Karamanakos, K. Pavlou, and S. Manias, "An enumeration-based model predictive control strategy for the cascaded H-bridge multilevel rectifier," *IEEE Trans. Ind. Electron.*, vol. 61, no. 7, pp. 3480–3489, Jul. 2014.

[14] P. Karamanakos, T. Geyer, N. Oikonomou, F. D. Kieferndorf, and S. Manias, "Direct model predictive control: A review of strategies that achieve long prediction intervals for power electronics," *IEEE Ind. Electron. Mag.*, vol. 8, no. 1, pp. 32–43, Mar. 2014.

[15] A. Ayad and R. Kennel, "Direct model predictive control of quasi-Z-source inverter compared with the traditional PI-based PWM control," in *Proc. Eur. Power Electron. Conf.*, Geneva, Switzerland, Sep. 2015, pp. 1–9.

[16] A. Ayad, P. Karamanakos, and R. Kennel, "Direct model predictive voltage control of quasi-Z-source inverters with *LC* filters," in *Proc. Eur. Power Electron. Conf.*, Karlsruhe, Germany, Sep. 2016, to appear, pp. 1–10.

[17] M. Mosa, R. Balog, and H. Abu-Rub, "High performance predictive control of quasi impedance source inverter," *IEEE Trans. Power Electron.*, DOI: 10.1109/TPEL.2016.2531989, to appear.

[18] A. Ayad, P. Karamanakos, and R. Kennel, "Direct model predictive current control of quasi-Z-source inverters," in *Proc. IEEE Int. Symp. Pred. Control of Elect. Drives and Power Electron.*, Valparaíso, Chile, Oct. 2015, pp. 1–6.

[19] E. L. Lawler and D. E. Wood, "Branch-and-bound methods: A survey," *Op. Res.*, vol. 14, no. 4, pp. 699–719, Jul./Aug. 1966.

[20] R. Cagienard, P. Grieder, E. C. Kerrigan, and M. Morari, "Move blocking strategies in receding horizon control," *J. of Process Control*, vol. 17, no. 6, pp. 563–570, Jul. 2007.

[21] P. Karamanakos, T. Geyer, and S. Manias, "Direct voltage control of dc-dc boost converters using enumeration-based model predictive control," *IEEE Trans. Power Electron.*, vol. 29, no. 2, pp. 968–978, Feb. 2014.